# Cavity effect on vertical and horizontal components of Rayleigh wave using 2D and 3D simulation models

**Hossein Rahnema**
Shiraz University of Technology
**Mehdi Hashemi Jokar**
Islamic Azad University of Shahrekord
**Mohammad Momeni**
Islamic Azad University of Shahrekord
**Meisam Mahboubi**
Shiraz University of Technology
**Sohrab Mirassi** ( s.mirasi@sutech.ac.ir )
Islamic Azad University of Shahrekord

**Research Article**

**Keywords:** Rayleigh wave, Radial and vertical components, Cavity, Finite Element Modeling (FEM), MASW

**Posted Date:** August 10th, 2022

**DOI:** https://doi.org/10.21203/rs.3.rs-1925836/v1

# Abstract

The potential risk of subsurface anomalies such as sinkhole and cavity has always been an important issue in geotechnical and geophysical engineering. Subsurface cavities have dissimilar effects on different components of Rayleigh wave in each direction. This paper intends to detect cavity and intrusion in the half-space and layered soil media. Rayleigh (R) wave propagation is analyzed according to the classical Multi-channel Analysis of Surface Waves (MASW) method. 2D and 3D simulations of Surface wave testing were conducted using Finite Element Modeling (FEM) in Abaqus 6.14. The results show the significant effect of the subsurface cavity on the particle motion and radial component of the Rayleigh wave. Cavity location is determined based on the variation of the maximum normalized amplitude for each trace. Furthermore, the perturbation of the elliptic shape above the cavity can help in cavity detection compared with the recorded data before and after the cavity.


# 1 Introduction

Subsurface anomalies such as cavities, sinkholes, weak subsurface layers, faults, tunnels, etc. may cause threats to humans [1–4]. The sinkhole phenomenon has particular importance, which is generally caused by factors such as groundwater level dropping and karst. Damages were appeared by sinkholes in various parts of the world, especially in the plains of Iran, e.g. in Surmagh plain (50 m in diameter and 16 m in depth), in Safashahr plain (50 m in width and 20 m in depth), in Kaboudarahang plain, Hamedan and the recently in Fassa plain (20 m in width and 100 m in depth) [5–8]. These subsurface cavities have caused serious damage to crop lands, residential buildings, roads and other structures as well as environmental, economic and social losses [5–8]. So, detection of sinkhole and cavity are really important for many engineering projects.

A multitude of studies have been dedicated to cavity detection by using seismic surface waves [9–13]. Shao et al. [14] studied near-surface cavity detection by generalized S-transform of Rayleigh (R) wave based on the small modification to the travel time equation for R-wave diffraction of the study of Xia et al. [10]. Chai et al. [3, 15] studied the influence of the source and void depth on the wave-field in half space and layered media by numerical simulation. For instance, Mi et al. [16] presented the horizontal resolution of the MASW method to recognize anomalies on a pseudo-2D shear wave velocity section. Attenuation analyses of R-wave have demonstrated satisfactory results in identifying shallow subsurface voids [9]. In addition, numerical studies [17–20] have verified the feasibility of detecting near-surface voids using seismic waves. Borisov et al. [21] also successfully applied 3D elastic full waveform inversion to detect voids in the near surface. Their results showed the ability of high-resolution 3D velocity models to detect the tunnel.

The main contribution of this paper is to apply the FEM method to identify cavities in soil media by analyzing the particles motions and different components of R-wave. The circular cavities are modeled in different materials of the empty cavity (cavity) and filled cavity (intrusion) in the half-space and layered soil media. The comparison of radial and vertical components of R-wave is conducted based on the

maximum normalized amplitude of each trace which is recorded by receivers. Furthermore, the particles motions of R-wave are evaluated in different location of receivers which are located before, above and after the buried cavity.

# 1.1 Methodology and Verification

In the finite element simulations, the reflection of waves into the medium is always observed due to the effect of seismic loading. Hereof, infinite elements were employed at the model boundaries. The infinite element method is not suitable for complex 2D and 3D modeling of surface wave propagations. In return, the Absorbing Layers using Increasing Damping (ALID) and Perfectly Matched Layer (PML) significantly reduce the geometrical and computational size of numerical models [22, 23]. Hence, simpler application of ALID in modeling as an absorbing boundary makes this method to be preferred [24, 25]. The thickness of ALID layers and the difference between adjacent layers damping affect the level of absorption and reflection of waves into the medium. As a result, high impedance differences between adjacent layers result in more reflection of waves into the medium. Therefore, in order to damp the waves at the boundaries of the model, an increasing-damping layout for the layers is used denoted by ALID. According to the analyses, a number of 20 ALID layers with thickness of 1 m are selected for more absorption of the reflected waves [26]. All models are simulated using FEM. For all models, the size of the model is 100 m × 50 m with considering the thickness of 20 m for absorbing boundary, at the bottom and both sides of the model. The sampling rate of 0.1 ms and acquisition time of 0.4 s are selected.

The synthetic shot was located of 1 m far from array. The generated waves were recorded with 48 m geophones array with a space of 1 m that were excited by a vertical source (50 Hz Ricker wavelet) as shown in the time and frequency domain in Fig. 1a. The source load function is given by Ricker wavelet [27, 28], which is expressed in the time domain as:

$$R(t) = \left(1 - 2\pi^2 f^2 t^2\right) e^{-\pi^2 f^2 t^2} \quad (1)$$

where $t$, $f$, and $R$ are time (s), frequency (Hz) and Ricker wavelet, respectively.

The results of recorded data of the geophones which are located on the surface are shown in Fig. 1b. This data are transferred from the time-offset domain to the frequency-wave number (f-k) domain. The results show that the maximum amplitude and energy obtained are related to the frequency of 10 Hz and the dominant frequency of the applied source load.

One layer model with shear wave velocity of 500 m/s is considered for verification of modeling results. As shown in Fig. 2, a homogeneous half-space soil model is employed to validate the software output and MATLAB analyses.

Based on the fact that VR ≈ 0.928×VS which is 462 m/s in the validation model, the Rayleigh wave dispersion curve of the homogeneous half-space model must also be obtained with the same velocity.

Figure 3(a) illustrates the wave-field recorded by the geophones in the time-offset domain (wave-field). R-waves with greater amplitudes and lower velocities can be identified clearly. The P-waves travel path also appears above the R-waves path with greater velocity or slighter slope. The phase velocity spectrum of the R-waves is illustrated in Fig. 3(b) representing an energy accumulation about the velocity of 462 m/s. By this, the reliability of FEM modeling and MATLAB analyses is validated.

# 2 Results And Discussion

In this paper, 2D and 3D simulations of single-layer (half-space) and layered soil media without cavity, with cavity and intrusion are considered. In this regard, particles motions (elliptic shape) of Rayleigh wave, the ratio and maximum normalized amplitude of the vertical and radial components of Rayleigh waves are investigated.

## 2.1 Rayleigh wave components in Half-space soil media (2D models)

The effect of a circular cavity and intrusion with a radius of 2.5 m in the homogeneous half-space model are investigated in this part. The general sketches of numerical models which are used for the simulation are illustrated in Fig. 4. In addition, the effect of this cavity (Fig. 4b) is compared with the results of half-space models without cavity (Fig. 4a) and with intrusion (Fig. 4c). The source load is located on the left side of the geophones array (forward). The circular cavity is located at the middle of 48 m geophone array at a distance of 24 m from the first geophone and also at the center of the first layer thickness [29]. The material properties of soil layers, cavity and intrusion for simulations are presented in Table 1. It must be underlined that the Basalt volcanic rock considered as a filled cavity (intrusion) and also for avoiding numerical difficulties the cavity with low elastic properties are used instead of the empty cavity [10].

Table 1
Material properties of soil media, cavity and intrusion

| Martial | Shear wave velocity(m/s) | P-wave velocity(m/s) | Elastic modulus (MPa) | Mass density (kg/m3) | Poisson's ratio | Rayleigh Damping ($\alpha$&$\beta$) |
|---|---|---|---|---|---|---|
| half-space | 500 | 866 | 1375 | 2200 | 0.25 | 0.83, 0.000085 |
| Cavity | 17 | 340 | 0.0086 | 10 | 0.498 | 3.2, 0.0009 |
| Intrusion (Volcanic rock) | 3000 | 5080 | 1.45E + 7 | 2400 | 0.338 | 0.23, 0.000031 |

As shown in Fig. 4, the cavity and intrusion are located below the center of the receiver array. It is expected to appear some changes in the amplitude of the horizontal and vertical components of the R-wave (elliptical shape of R-wave) due to the presence of subsurface cavities. The recorded data by 49 receivers for a half-space model without and with cavity are illustrated in Fig. 5a and 5b, respectively. By comparing the obtained results, the effects of cavity on the particles motions of R-wave can be identified in the central receivers (around the 24th receiver) as shown in Fig. 5b. Hence, the deformed shapes of particles motions in some receivers indicate the influence of the cavity on different components of R-wave.

The comparative results of half-space soil model without cavity and with cavity and intrusion are represented in Fig. 6, Fig. 7 and Fig. 8, respectively. The elliptical shape of R-wave for all three locations of recorded data by the receiver are the same in soil media without cavity. On the other hand, for the soil media with cavity and intrusion, the effect of cavity and intrusion can be identified based on the deformation of the elliptical shape of R-wave which is recorded by geophones above the cavity and intrusion (Fig. 7b and 8b). It should be mentioned that, there are not any significant changes in the elliptical shape of R-wave which is recorded before and after the location of the cavity and intrusion as shown in Fig. 7a, 7c, 8a and 8c.

The aforementioned results demonstrate that the radial and vertical components of R-wave can represent the effect of subsurface cavity. In this regard, the comparison of radial and vertical components of R-wave are conducted based on the maximum normalized amplitude of each trace. It means, the maximum normalized amplitude of each trace is determined and then all these values for each receiver are shown in Fig. 9a and 10a. The significant sharp changes of different components of R-wave represent the location of cavity around the 24th receiver. Furthermore, the radial to vertical and vertical to radial ratio are shown in Fig. 9b and 10b which the location and effect of cavity are detectable. The effects of intrusion on the maximum normalized amplitude and different component ratio are more clear due to the great differences between the elastic modulus of intrusion and soil media. So, according to the obtained results, the cavity and intrusion could be detected by using maximum normalized amplitude and ratio of different components.

## 2.2 Rayleigh wave components in layered soil media (2D models)

In this section, the two-layer soil models are evaluated with the first layer 40 m thick and the second layer (half-space) 60 m thick. As illustrated in Fig. 11, the circular cavity and intrusion with a radius of 2.5 m are located at the center of receiver array and the Ricker source load with central frequency of 50 Hz is applied on the left side of receivers. Similar to the previous part process, the obtained results of soil model with cavity are compared with the models without cavity and with intrusion (Fig. 11). The material properties of two-layer soil models and simulations are presented in Table 1.

Table 2
Material properties of soil media, cavity and intrusion

| Martial | Shear wave velocity(m/s) | P-wave velocity(m/s) | Elastic modulus (MPa) | Mass density (kg/m3) | Poisson's ratio | Rayleigh Damping ($\alpha$&$\beta$) |
|---|---|---|---|---|---|---|
| First layer | 200 | 400 | 192 | 1800 | 0.33 | 1.67, 0.00017 |
| half-space | 500 | 866 | 1375 | 2200 | 0.25 | 0.83, 0.000085 |
| Cavity | 17 | 340 | 0.0086 | 10 | 0.498 | 3.2, 0.0009 |
| Intrusion (Volcanic rock) | 3000 | 5080 | 1.45E + 7 | 2400 | 0.338 | 0.23, 0.000031 |

The results of two-layer soil models without cavity and with cavity and intrusion are illustrated in Fig. 12. The comparative curves of the maximum normalized amplitude of vertical and radial components are presented in the first column of Fig. 12. By comparing the results of soil models with cavity and intrusion with soil model without cavity, it could be identified the location of cavity and intrusion based on the significant sharp changes which are appeared around the 24th receiver (Fig. 12c and 12e). Furthermore, the ratio of different components of R-wave for soil models with cavity and intrusion could be helpful to find the effect of subsurface cavity (Fig. 12d and 12f). It should be noted that the vertical to radial ratio represents more significant changes compared to radial to vertical ratio. So, it could be inferred that some local changes in the amplitude of different components of R-wave and their ratio are related to the presence of cavity and intrusion.

# 2.3 Rayleigh wave components in layered soil media (3D models)

The circular cavity with a radius of 2.5 m and a central depth of 3.5 meters from the ground surface is considered in 3D model as shown in Fig. 13. Similar to the previous section, Ricker source load with a central frequency of 50 Hz is applied on the left side of the receivers. The vertical and horizontal components of R-wave are recorded to identify the subsurface cavity by using 3D modeling in Abaqus software.

The obtained results from 3D simulations are shown in Fig. 14. The local changes in the maximum normalized amplitude curves of R-wave components are presented in Fig. 14-a, which clearly show the effect of the subsurface cavity on the vertical component and especially on the radial component of R-waves. In addition, the location of cavities can be clearly seen in Fig. 14-b according to the ratio of the radial to the vertical component of R-waves (R/V). It can be stated that the location of subsurface cavity can be determined with higher accuracy by using the ratio of the Rayleigh wave components (Fig. 17- b). It should be noted that the amplitude changes of the radial component have a greater intensity than the vertical amplitude of R-wave

# 3 Conclusion

This paper represents the results of numerical studies to identify subsurface cavity and intrusion in half-space and layered soil media. The maximum normalized amplitude and different components ratio of Rayleigh waves were evaluated to detect cavity and intrusion. Also, the elliptical shape of R-wave for all three locations (before, above and after the cavity) of data recorded by the receivers were compared. By comparing the results obtained for without and with cavity and intrusion conditions, it was observed that some local changes in the maximum normalized amplitude and the ratio of different components of R-wave were related to the presence of cavity and intrusion. Also, the deformation of the elliptical shape of R-wave represented the location of the cavity and intrusion. In general, elliptical shape of particle motions, the maximum normalized amplitude of each trace, and the ratio of different components of Rayleigh wave were found to be helpful in detecting of cavities by using synthetic data.

# Declarations

### Conflicts of interest

On behalf of all authors, the corresponding author states that there is no conflict of interest.

# References


1. Rahnema H, Mirassi S, Dal Moro G (2021) Cavity effect on Rayleigh wave dispersion and P-wave refraction. Earthq Eng Eng Vib 20(1):79–88
2. Rahnema H, Moradi M, Mirassi S (2022) 'Detecting the depth and thickness of weak layer in soil media using phase velocity spectrum and theoretical dispersion curve of Rayleigh wave'. Iran J Geophys. (), pp. -. doi: 10.30499/ijg.2022.322583.1389
3. Chai HY, Goh SH, Phoon KK, Wei CF, Zhang DJ (2014) Effects of source and cavity depths on wave fields in layered media. J Appl Geophys 107:163–170
4. Shaaban F, Ismail A, Massoud U, Mesbah H, Lethy A, Abbas AM (2013) Geotechnical assessment of ground conditions around a tilted building in Cairo–Egypt using geophysical approaches. J Association Arab Universities Basic Appl Sci 13(1):63–72
5. Rahnema H, Mirassi S (2014) Drought and water crisis in Plains of Iran: a case study of Marvdasht and Khanmirza Plains, Fars and Chaharmahal and Bakhtiari Province, Iran.International Bulletin of Water Resources and Development, 2(1), pp.139 – 54.
6. Rahnema H, Mirasi S (2012) Seismic and geotechnical study of land subsidence and vulnerability of rural buildings. Int J Geosci 3(04):878
7. Rahnema H, Mirassi S (2016) Study of land subsidence around the city of Shiraz. Scientia Iranica. Transaction A, Civil Engineering, 23(3), p.882
8. Rahnema H, Mirassi S (2014) Crisis management concerning underground water falling and land subsidence occurrence in the plains of Iran. Advances in Environmental Biology, pp 1453–1466

9. Nasseri-Moghaddam A, Cascante G, Hutchinson J (2005) A new quantitative procedure to determine the location and embedment depth of a void using surface waves. J Environ Eng Geophys 10(1):51–64
10. Xia J, Nyquist JE, Xu Y, Roth MJ, Miller RD (2007) Feasibility of detecting near-surface feature with Rayleigh-wave diffraction. J Appl Geophys 62(3):244–253
11. [Xia J, Xu Y, Luo Y, Miller RD, Cakir R, Zeng C (2012) Advantages of Using Multichannel Analysis of Love Waves (MALW) to Estimate Near-Surface Shear-Wave Velocity. Surv Geophys 33:841–860
12. Mirassi S, Rahnema H (2020) Deep cavity detection using propagation of seismic waves in homogenous half-space and layered soil media. Asian J Civ Eng 21:1431–1441. https://doi.org/10.1007/s42107-020-00288-2
13. Rahnema H, Rasekh M, Mirassi S (2021) 'Effect of subsurface cavity length on Rayleigh wave propagation to identify near and far boundary of the cavity'. J Struct Constr Eng. (), pp. -. doi: 10.22065/jsce.2021.299727.2530
14. Shao GZ, Tsoflias GP, Li CJ (2016) Detection of near-surface cavities by generalized S-transform of Rayleigh waves. J Appl Geophys 129:53–65
15. Chai HY, Phoon KK, Goh SH, Wei CF (2012) Some theoretical and numerical observations on scattering of Rayleigh waves in media containing shallow rectangular cavities. J Appl Geophys 83:107–119
16. Mi B, Xia J, Shen C, Wang L, Hu Y, Cheng F (2017) Horizontal resolution of multichannel analysis of surface waves. Geophysics 82(3):EN51–EN66
17. Gelis C, Leparoux D, Virieux J, Bitri A, Operto S, Grandjean G (2005) Numerical modeling of surface waves over shallow cavities. J Environ Eng Geophys 10:111–121
18. Nasseri-Moghaddam A, Cascante G, Phillips C, Hutchinson DJ (2007) Effects of underground cavities on Rayleigh waves-Field and numerical experiments. Soil Dyn Earthq Eng 27(4):300–313
19. Wang D, Wang M, Li J, Feng S (2014) Ground surface response induced by shallow buried explosions. Earthq Eng Eng Vib 13(1):163–169
20. Hei B, Yang Z, Chen Z (2016) Scattering of shear waves by an elliptical cavity in a radially inhomogeneous isotropic medium. Earthq Eng Eng Vib 15(1):145–151
21. Borisov D, Modrak R, Gao F, Tromp J (2017) 3D elastic full-waveform inversion of surface waves in the presence of irregular topography using an envelope-based misfit function. Geophysics 83(1):R1–R11
22. Davoodi M, Pourdeilami A, Jahankhah H, Jafari MK (2018) Application of perfectly matched layer to soil-foundation interaction analysis. *Journal of Rock Mechanics and Geotechnical Engineering*
23. Rajagopal P, Drozdz M, Skelton EA, Lowe MJ, Craster RV (2012) On the use of absorbing layers to simulate the propagation of elastic waves in unbounded isotropic media using commercially available finite element packages. NDT & E International 51:30–40

24. Lin S, Ashlock JC (2016) Surface-wave testing of soil sites using multichannel simulation with one-receiver. Soil Dyn Earthq Eng 87:82–92
25. Lin S, Ashlock JC (2014) Multimode Rayleigh wave profiling by hybrid surface and borehole methods. Geophys J Int 197(2):1184–1195
26. Mirassi S, Rahnema H (2020) 'Improving the performance of absorbing layers with increasing damping in the numerical modeling of surface waves propagation using finite element method'. Sci Q J Iran Association Eng Geol 13(2):13–26
27. Zhang N, Gao Y, Li D, Wu Y, Zhang F (2012) Scattering of SH waves induced by a symmetrical V-shaped canyon: a unified analytical solution. Earthq Eng Eng Vib 11(4):445–460
28. Rahnema H, Mirassi S (2021) 'Effect of frequency content of seismic source load on Rayleigh and P waves in soil media with cavity'. J Struct Constr Eng 8(2):280–300. doi: 10.22065/jsce.2019.176403.1808
29. Mirassi S, Rahnema H (2021) 'Effect of acquisition parameters on the resolution of dispersion image in multi-channel analysis of surface wave method'. Sharif J Civil Eng 362(41):3–13. doi: 10.24200/j30.2019.53491.2551

# Figures

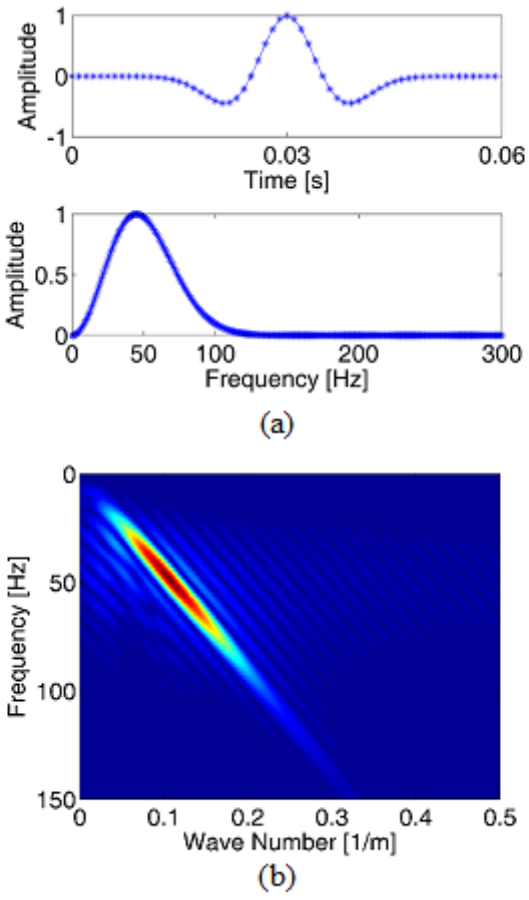

## Figure 1

Ricker source load with 50 Hz central frequency: a) Frequency-wavenumber spectrum of recorded data from the FEM model; b) shape of the source in time and frequency domain

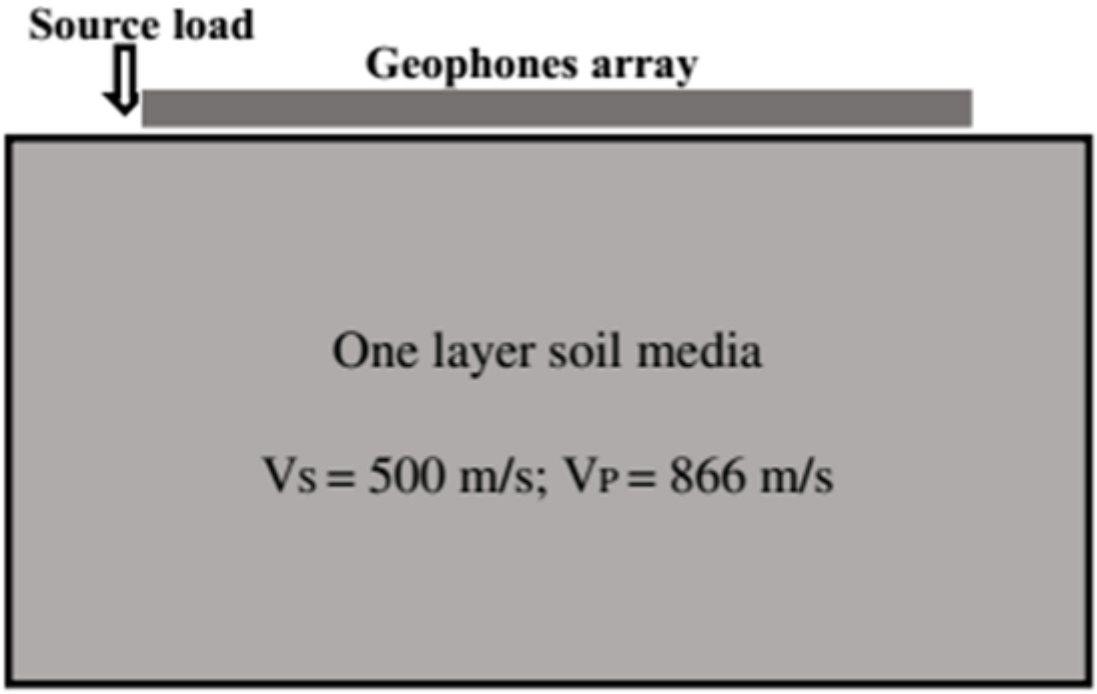


## Figure 2

2D plain strain of one-layer (half-space) soil model for verification

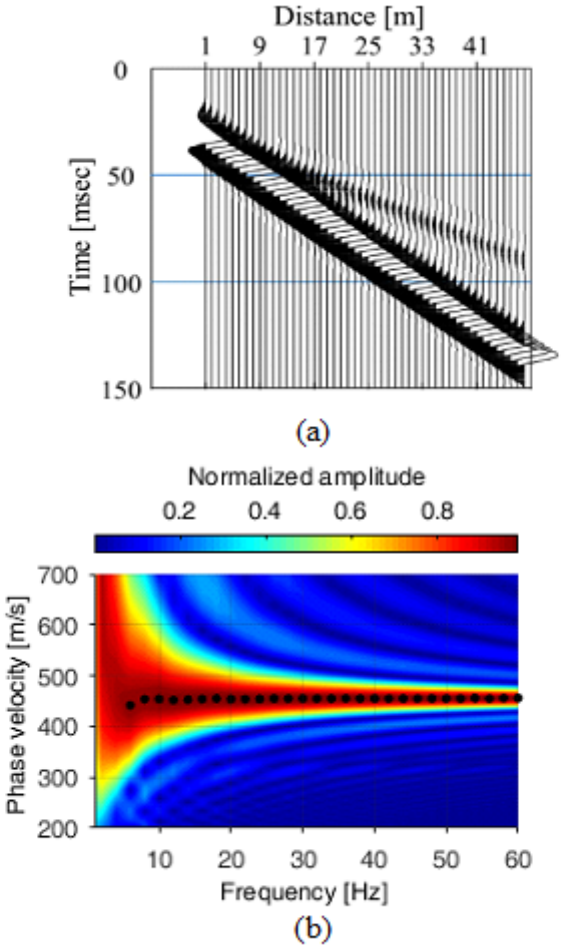


## Figure 3

Synthetic results of one layer model: (a) Normalized seismic traces in the time-offset domain; (b) velocity spectrum and dispersion curve

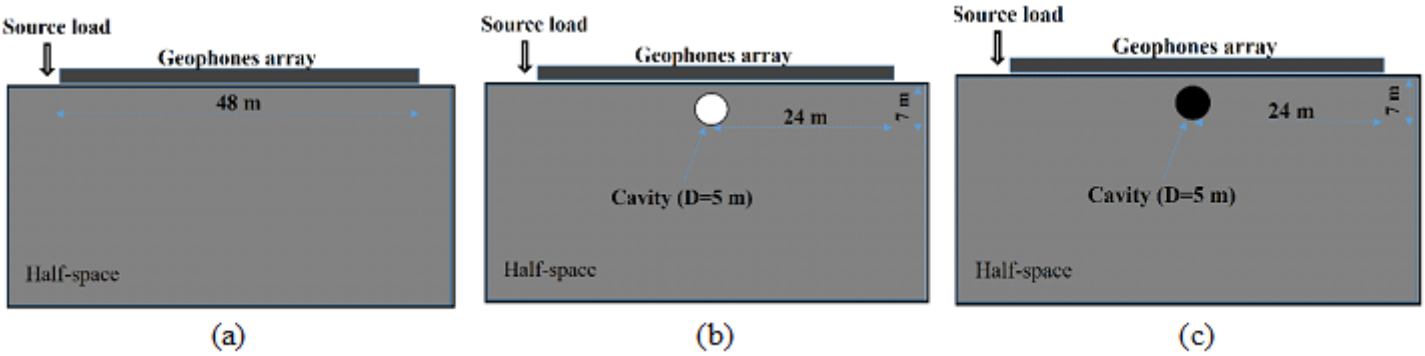


## Figure 4

Half-space soil models: a) without cavity; b) with cavity; c) with intrusion.

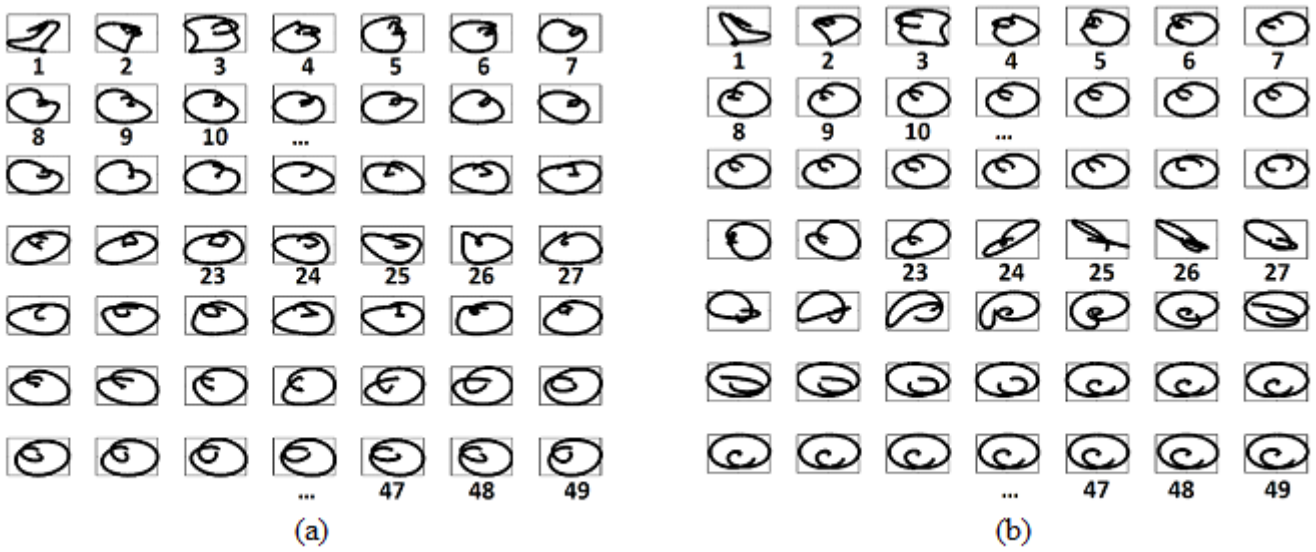


## Figure 5

Recorded Particles motions (elliptic shape) of Rayleigh wave at each geophone (49 geophones) for half-space soil media with and without a cavity

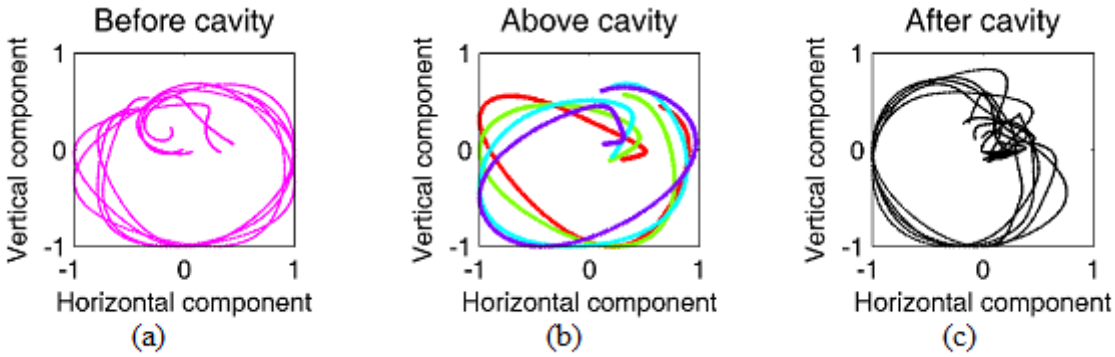


## Figure 6

Particles motions of Rayleigh wave at different locations in the half-space soil media without cavity

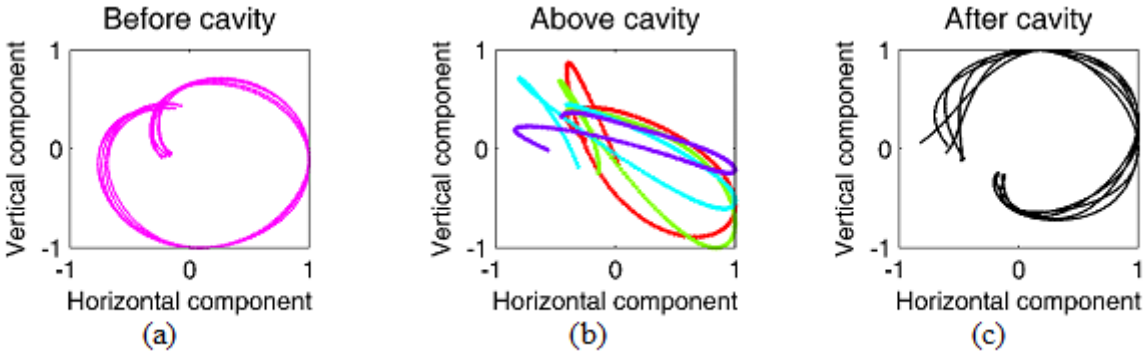


**Figure 7**

Particles motions of Rayleigh wave at different locations: before, above and after the cavity in the half-space soil media with cavity

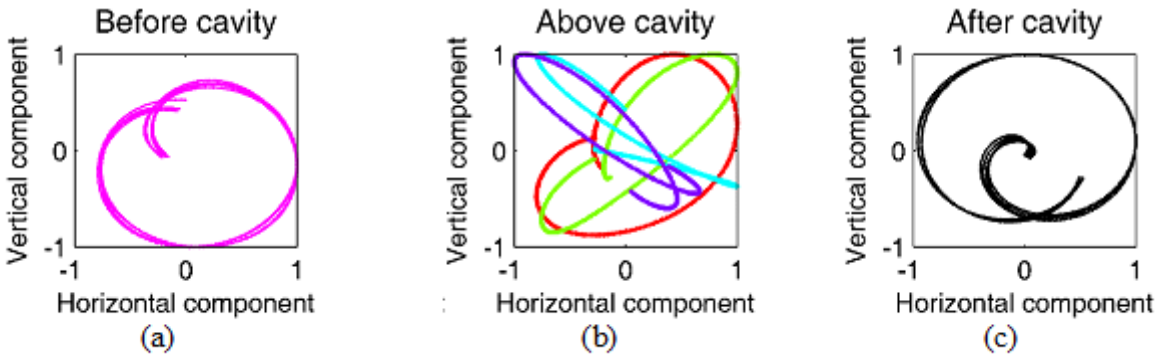


**Figure 8**

Particles motions of Rayleigh wave at different locations: before, above and after the intrusion in the half-space soil media with intrusion

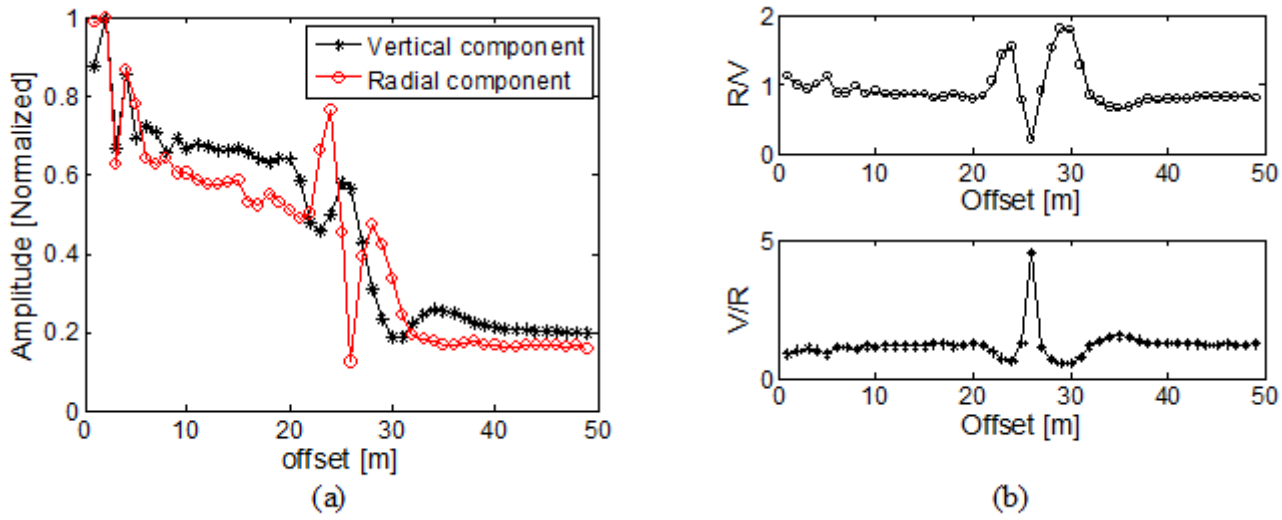


**Figure 9**

results of half-space modeling with cavity: a) maximum normalized amplitude of radial and vertical components of R-wave; b) radial to vertical and vertical to radial ratio

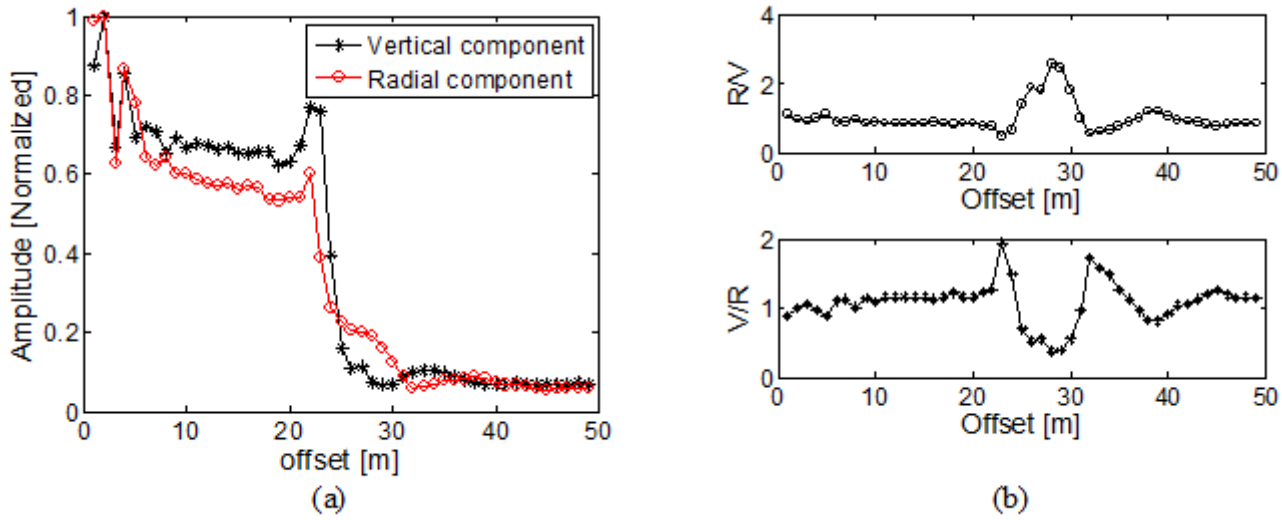


**Figure 10**

results of half-space modeling with intrusion: a) maximum normalized amplitude of radial and vertical components of R-wave; b) radial to vertical and vertical to radial ratio

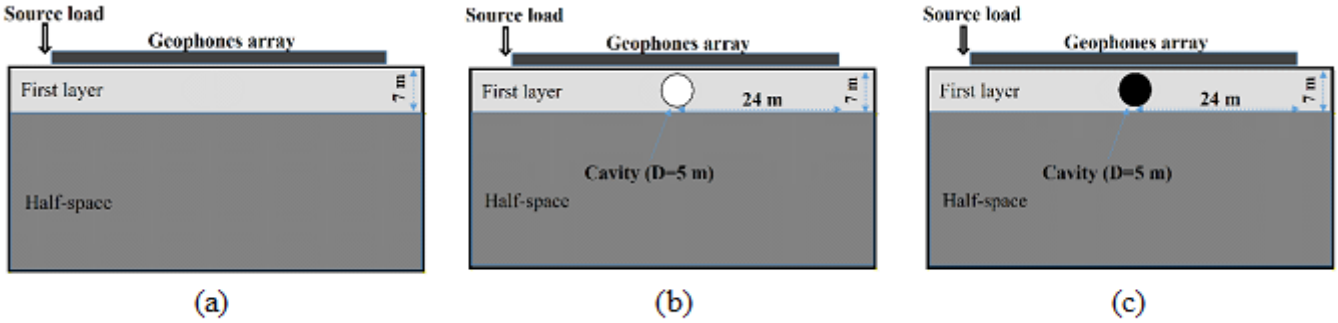


## Figure 11

Two-layer soil models: a) without cavity; b) with cavity; c) with intrusion

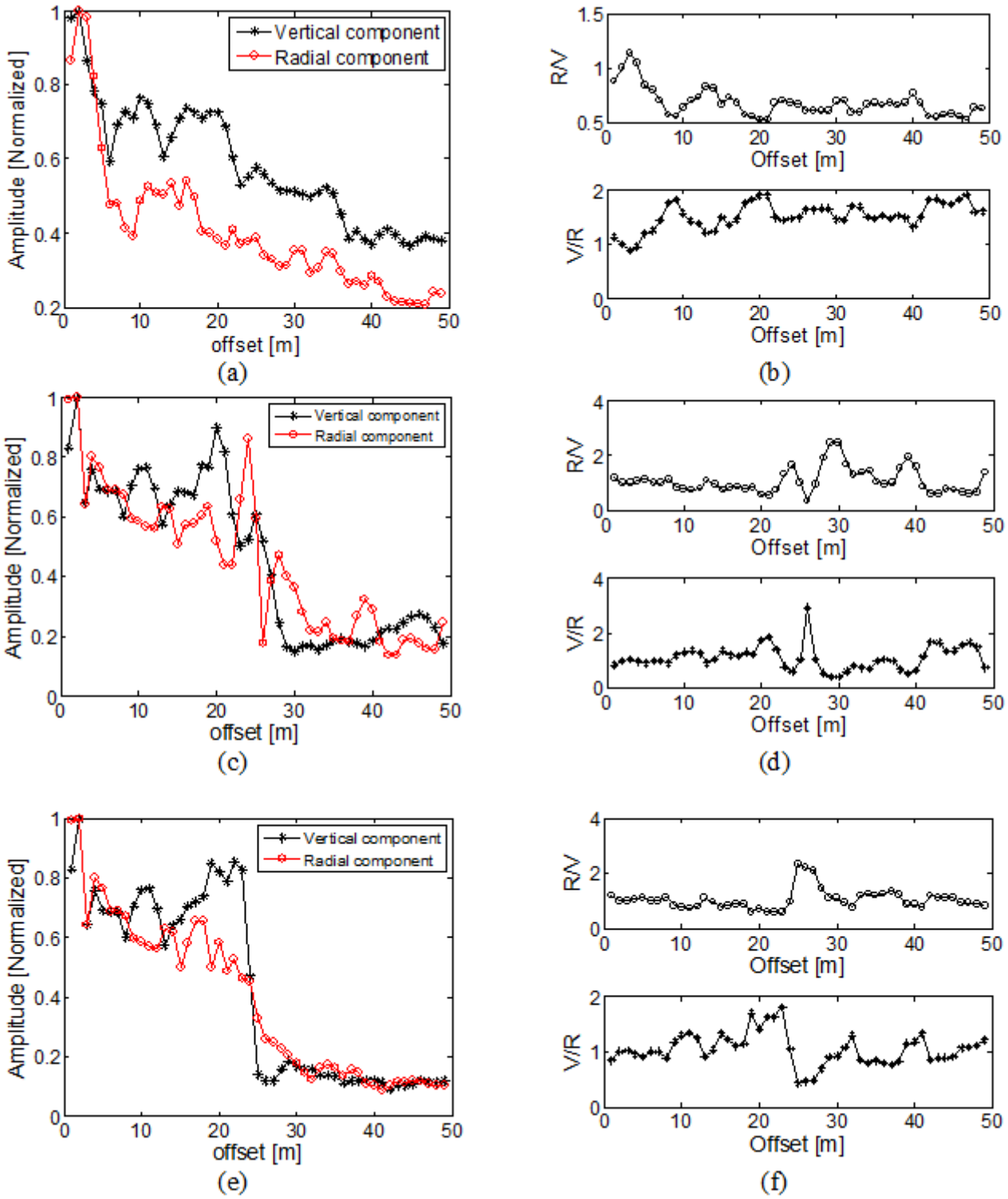


## Figure 12

comparing the maximum normalized amplitude and different component ration of R-wave in the first and second column,

respectively for two-layer modeling: a, b) without cavity; c, d) with cavity; e, f) with intrusion

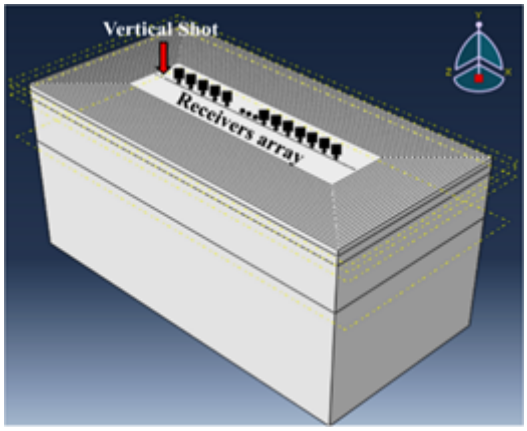


**Figure 13**

View of the 3D model with seismic source load

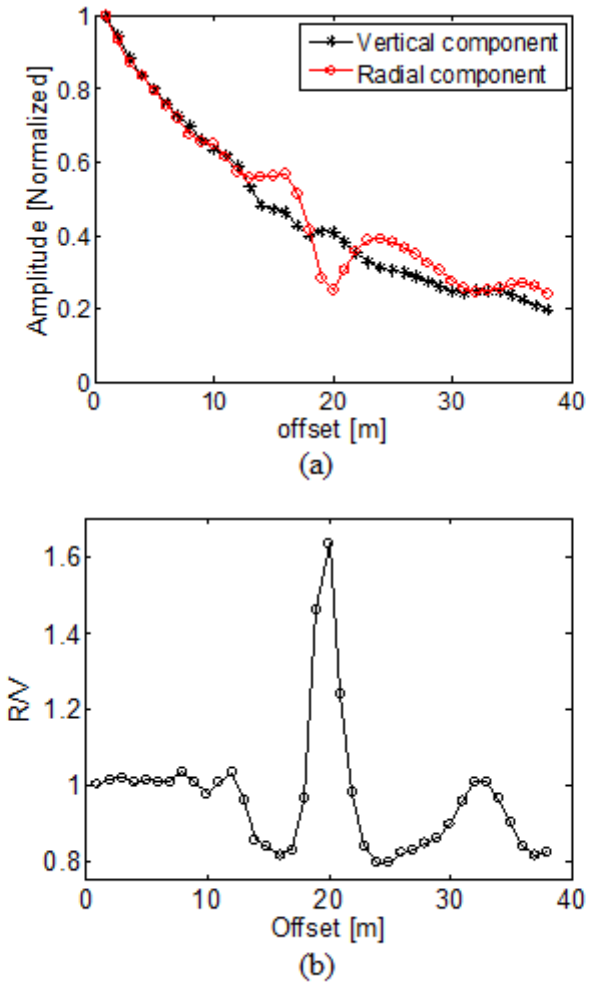


**Figure 14**

The results of the normalized maximum amplitude of the vertical and radial components of R-waves: a) Comparison of maximum normalized amplitude; b) The ratio of vertical and radial components of R-waves